# We are IntechOpen, the world's leading publisher of Open Access books Built by scientists, for scientists

6,900
Open access books available

186,000
International authors and editors

200M
Downloads

Our authors are among the

154
Countries delivered to

TOP 1%
most cited scientists

12.2%
Contributors from top 500 universities


WEB OF SCIENCE™

Selection of our books indexed in the Book Citation Index in Web of Science™ Core Collection (BKCI)

## Interested in publishing with us?
## Contact book.department@intechopen.com

Numbers displayed above are based on latest data collected.
For more information visit www.intechopen.com

Chapter 8

# Mesoscopic Physics of Phonon Transport in Carbon Materials

Kenji Sasaoka and Takahiro Yamamoto

Additional information is available at the end of the chapter

http://dx.doi.org/10.5772/intechopen.81292

**Abstract**

We give a theoretical review of recent development of the mesoscopic physics of phonon transport in carbon nanotubes, including the quantization of phonon thermal conductance, phonon Anderson localization, and so on. A single-walled carbon nanotube (SWCNT) can be regarded as a typical one-dimensional phonon conductor and exhibits various interesting phenomena originating from its one dimensionality. For example, a pristine SWCNT without any defects shows the quantization of phonon thermal conductance at low temperature. On the other hand, a defective SWCNT with randomly distributed carbon isotopes shows the phonon Anderson localization originating from the interference between phonons scattered by isotope impurities.

**Keywords:** carbon nanotube, ballistic phonon, quantized thermal conductance, phonon Anderson localization, phonon waveguide

## 1. Introduction

Heating of electronic devices is an unavoidable serious problem toward the realization of next-generation nanoscale devices. Carbon nanotube (CNT) is expected to be a potential material for removing the heat from heated devices because of its high thermal conductivity. However, concern has been raised that intrinsic high thermal conductivity of pure CNTs is lost because of the presence of defects in synthesized CNTs.

In this chapter, we give a review of recent progress of theoretical works on phonon transport in CNTs focusing on the quantization of phonon thermal conductance, phonon Anderson localization, and so on. The phonon transport in CNTs shows fully quantum behaviors at low

IntechOpen

© 2018 The Author(s). Licensee IntechOpen. This chapter is distributed under the terms of the Creative Commons Attribution License (http://creativecommons.org/licenses/by/3.0), which permits unrestricted use, distribution, and reproduction in any medium, provided the original work is properly cited. CC BY

temperatures and exhibits strong nonlinear behaviors due to phonon-phonon interaction at high temperatures. Therefore, traditional transport theories for bulk objects are not applicable to the thermal transport in CNTs. In the chapter, we will introduce a novel theory for mesoscopic phonon transport we developed and will describe various results and their physical interpretations.

## 2. Coherent phonon thermal transport in carbon nanotubes

### 2.1. Quantized thermal conductance of carbon nanotubes

In the one-dimensional (1D) phonon system formed between heat and cold baths, the thermal current density is described as the Landauer energy flux [1–3], which is given by

$$\dot{Q}_{\mathrm{ph}} = \sum_m \int_0^\infty \frac{dk}{2\pi} \hbar\omega_m(k) v_m(k) [\eta(\omega_m, T_{\mathrm{hot}}) - \eta(\omega_m, T_{\mathrm{cold}})] \zeta_m(k) \tag{1}$$

where $\hbar\omega_m(k)$ a phonon energy dispersion of wave number $k$ and a phonon mode index $m$, $v_m(k) = d\omega_m(k)/dk$ a group velocity, $\eta(\omega_m, T_\alpha) = \left[\exp\left(\hbar\omega_m(k)/k_B T_\alpha\right) - 1\right]^{-1}$ the Bose-Einstein distribution function in heat baths, and $\zeta_m(k)$ is the transmission probability between the system and heat baths [1].

Analytically, performing the integration in Eq. (1) is, generally, very difficult, and it requires a knowledge of $\omega_m(k)$ and $\zeta_m(k)$ as a function of $m$ and $k$. However, transformation of the integration variable in Eq. (1) from $k$ to $\omega_m(k)$ leads to a cancelation between $v_m(k)$ and the density of state, $dk/d\omega_m$, so that Eq. (1) is rewritten as

$$\dot{Q}_{\mathrm{ph}} = \sum_m \int_{\omega_m^{\min}}^{\omega_m^{\max}} \frac{d\omega_m}{2\pi} \hbar\omega_m [\eta(\omega_m, T_{\mathrm{hot}}) - \eta(\omega_m, T_{\mathrm{cold}})] \zeta_m(\omega_m) \tag{2}$$

Here $\omega_m^{\min}$ and $\omega_m^{\max}$ are the minimum and maximum angular frequencies of the $m$th phonon dispersion, respectively. It is noted that Eq. (2) depends on only $\omega_m^{\min}$ and $\omega_m^{\max}$ regardless of the energy dispersion. Furthermore, within the linear response limit, $\Delta T \equiv T_{\mathrm{hot}} - \mathrm{T}_{\mathrm{cold}} \ll T \equiv (T_{\mathrm{hot}} + T_{\mathrm{cold}})/2$, and the limit of adiabatic contact between the system and heat baths, $\zeta_m(\omega_m) = 1$, the thermal conductance, $\kappa_{\mathrm{ph}} = \dot{Q}_{\mathrm{ph}}/\Delta T$, is simplified as

$$\kappa_{\mathrm{ph}} = \frac{k_{\mathrm{B}}^2 T}{2\pi\hbar} \sum_m \int_{x_m^{\min}}^{x_m^{\max}} dx \frac{x^2 e^x}{(e^x - 1)^2} \tag{3}$$

Carrying out the integration in Eq. (3), we can derive an analytical expression of the thermal conductance, which can easily apply to various 1D ballistic phonon systems, $\kappa_{\mathrm{ph}} = \kappa_{\mathrm{ph}}^{\min} - \kappa_{\mathrm{ph}}^{\max}$:

http://dx.doi.org/10.5772/intechopen.81292

$$\kappa_{\mathrm{ph}}^{\alpha} = \frac{2k_{\mathrm{B}}^2 T}{h} \sum_m \left[ \phi\left(2, e^{-x_m^{\alpha}}\right) + x_m^{\alpha} \phi\left(1, e^{-x_m^{\alpha}}\right) + \frac{\left(x_m^{\alpha}\right)^2}{2} \eta\left(x_m^{\alpha}\right) \right] \tag{4}$$

Here, $\alpha$ denotes "min" or "max," $\phi(z,s) = \sum_{n=1}^{\infty} (s^n/n^z)$ is the Appel function, and $x_m^{\alpha} = \hbar\omega_m^{\alpha}/k_{\mathrm{B}}T$. In particular, an acoustic mode ($\omega_m^{\min} = 0$) contributes a universal quantum of $\kappa_0 = \pi^2 k_{\mathrm{B}}^2 T/3h$ to the thermal conductance.

The thermal conductance in single-walled carbon nanotubes (SWCNTs) can be obtained by knowing the values of $\omega_m^{\min}$ and $\omega_m^{\max}$ for all $m$. These values can be obtained from the diagonalization of the dynamical matrix, constructed with the scaled force-constant parameters [4, 5]. **Figure 1** shows energy dispersion curves for the region near $k = 0$ for a CNT with chiral vector $\boldsymbol{C}_{\mathrm{h}} = (10, 10)$, where $|\boldsymbol{T}|$ is the magnitude of the unit vector along the tube axis. Here, the chiral vector$(n, m)$ uniquely determines the geometrical structure of CNTs [5, 7]. **Figure 1** shows four acoustic modes with linear dispersion: a longitudinal acoustic one, doubly degenerate transverse acoustic ones, and a twisting one. The lowest doubly degenerate optical ($E_{2g}$ Raman active) modes have an energy gap of $\hbar\omega_{\mathrm{op}} = 2.1$ meV at $k = 0$. As shown in the inset of **Figure 1**, $\hbar\omega_{\mathrm{op}}$ depends only on the tube radius $R$ and decreases approximately according to $\sim 1/R^2$ [5, 7]. These modes always lie in low-energy dispersion relations, independent of the geometry of SWCNTs.

**Figure 2(a)** shows the thermal conductances normalized to a universal value of $4\kappa_0$ (as explained later) as a function of temperature. The calculated values approach unity in the

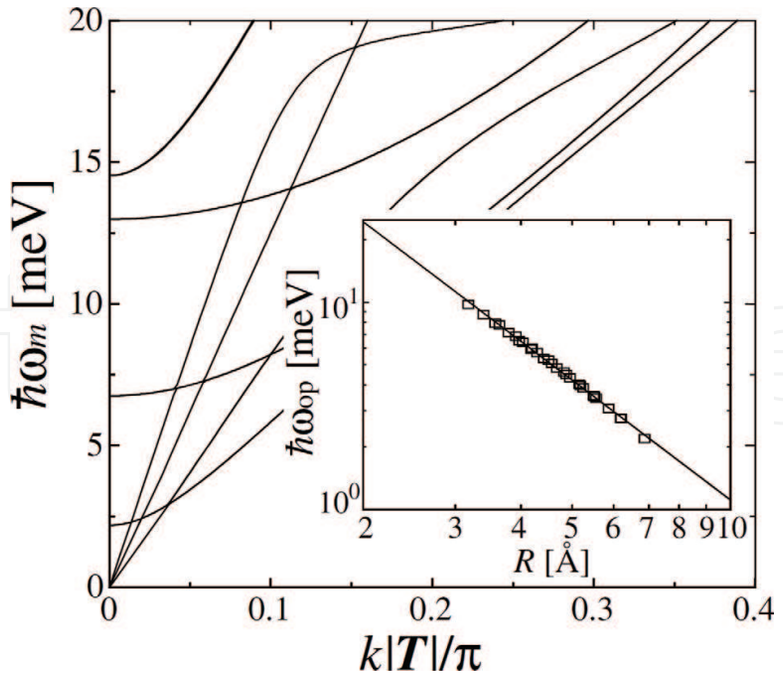


**Figure 1.** Low-energy phonon dispersion curves for a (10,10) SWCNT [6]. The inset shows the energy gap of the lowest optical modes. Copyright 2004 American Physical Society.

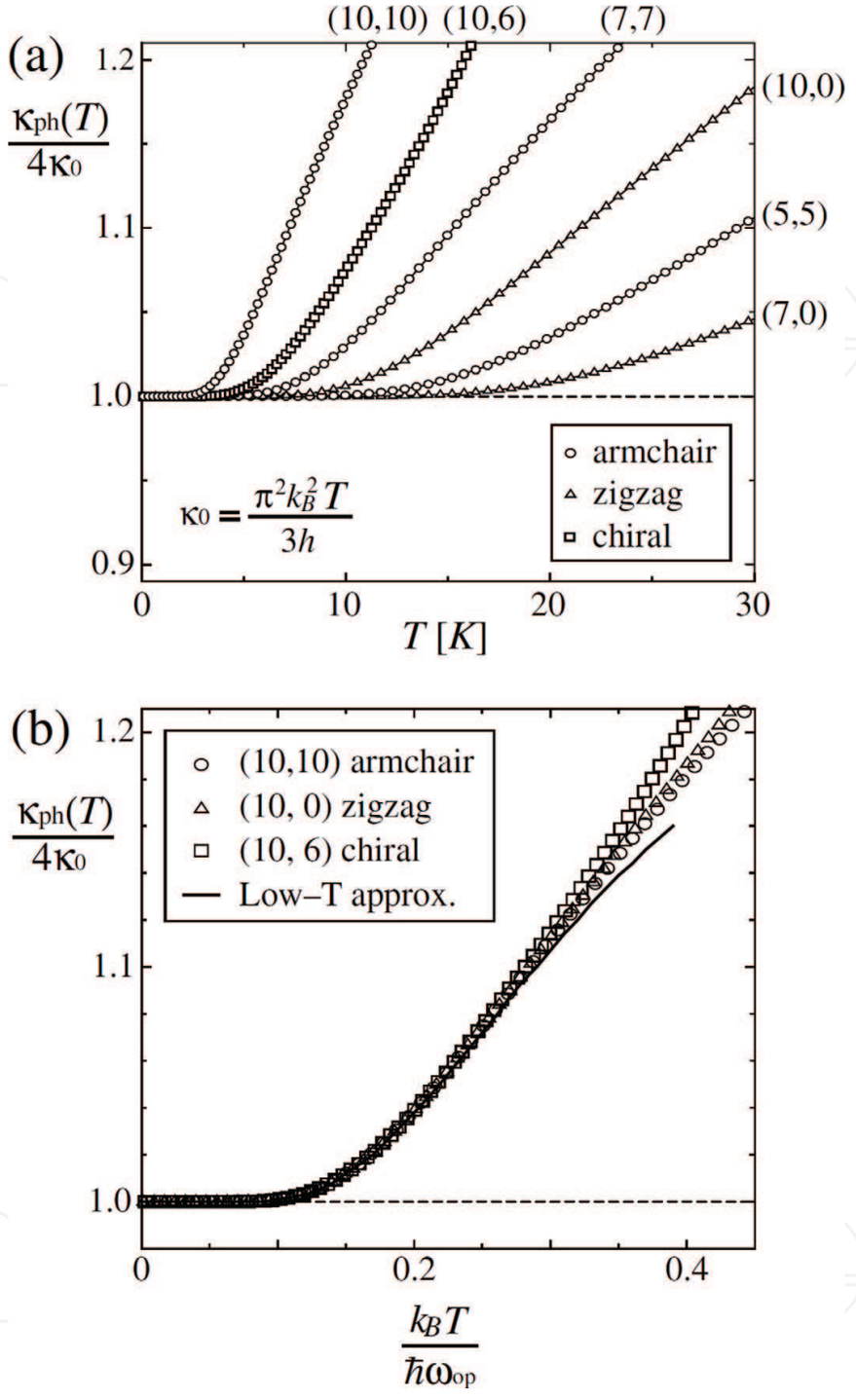


**Figure 2.** Thermal conductance as a function of temperature (a) in units of Kelvin and (b) scaled by the energy gap of the lowest optical mode [6]. Copyright 2004 American Physical Society.

low-temperature limit, meaning that the phonon thermal conductance of SWCNTs is quantized in unit of a universal value of $4\kappa_0$, independent of the chirality of SWCNTs. The origin of the quantization of thermal conductance is low-energy excitations of long wavelength acoustic phonons (four branches in **Figure 1**) at temperatures sufficiently low that the two lowest optical modes with $\hbar\omega_{op}$ are not excited (lowest gapped branch in **Figure 2**). The quantization

can also be derived analytically from Eq. (4). Only the first term contributes to the conductance at the low-$T$ limit, leading to $4\left(\pi^2 k_B^2 T/3h\right) = 4\kappa_0$. Here, 4 is the number of acoustic branches.

As another important finding, the different curves of $\kappa_{ph}(T)$ for various SWCNTs seen in **Figure 2(a)** exhibit a universal feature when a scaled temperature is introduced, $\tau_{op} = k_B T/\hbar\omega_{op}$. Taking account of the four acoustic and two lowest optical modes and substituting the values of $\omega_m^{min}$ for these branches at the $k = 0$ into Eq. (2), the thermal conductance can be given as

$$\frac{\kappa_{ph}}{4\kappa_0} \approx 1 + \frac{3}{\pi^2} e^{-1/\tau_{op}} \left(1 + \frac{1}{\tau_{op}} + \frac{1}{2\tau_{op}^2}\right) \tag{5}$$

The curves in **Figure 2(a)** are replotted against the curve of Eq. (5) with $\tau_{op}$ in **Figure 2(b)**. It is evident that all curves (only three curves are shown for clarity) fall on a single curve coinciding with the curve of Eq. (5) in the low-$T$ limit. The curves turn upward at around $\tau_{op} \approx 0.14$ from a linear region in this plot (quantization plateau), with the plateau width determined by the relation $\sim 1/R^2$ (see result in the inset of **Figure 1**). This universal feature of $\kappa_{ph}(T)$ of SWCNTs indicates that the optical phonon energy gap, which is decided only by $R$, characterizes low-temperature phonon transport, as shown in the inset of **Figure 1**. This theoretical result supports both the experimental observations and the inferred tube-radius dependence of the width of the thermal conductance plateau, although the unknown extrinsic factors in the experiment makes it impossible to compare the absolute values between the experiment and theory directly [8, 9].

The contribution of electrons to thermal conductance can be determined in a simple manner by replacing $\eta(\omega_m, T)$ in Eq. (1) with $f(\epsilon_m, T) = 1/\left[e^{(\epsilon_m - \mu)/k_B T} + 1\right]$ and then substituting the electron energy bands, $\epsilon_m$, into the formula. According to this formulation, all conduction bands crossing the Fermi energy level yield $\kappa_0$, as that of phonons, even though electrons obey different statistics. Generally, the quantum of thermal conductance should be universal out of relation to particle statistics [1, 10].

The low-$T$ behavior of the electronic thermal conductance in SWCNTs is dependent on whether the SWCNT is metallic or semiconducting, which is sensitive to radius and chirality [11, 12]. For semiconducting SWCNTs, the electronic thermal conductance, $\kappa_{el}$, should vanish roughly exponentially in the limit of $T \to 0$, having an energy gap of the order of 0.1 eV [13–15]. For metallic SWCNTs, two linear energy bands crossing the Fermi level at $k > 0$ [5] contribute to$\kappa_{el}$ at low temperatures, resulting in a universal value of $\kappa_{el} = 4\kappa_0$, where 4 is the number of two spin-degenerate channels crossing the Fermi level. This result also satisfies the Wiedemann-Franz relation between electrical conductance and electronic thermal one [16–18]. The total thermal conductance of metallic SWCNTs is given by $\kappa = \kappa_{el} + \kappa_{ph} = 8\pi^2 k_B^2 T/3h$ at low temperatures.

Finally, in this subsection, a significant difference was recognized between the widths of the quantization plateau for phonons and those for electrons in metallic SWCNTs. The characteristic

energy for phonon transport at low temperature is $\hbar\omega_{\mathrm{op}}$, typically a few meV, as described in **Figure 2(b)**, while that for electron transport is of the order of 0.1 eV, which corresponds to the energy at a Van Hove singularity measured from the Fermi level [19]. As a result, it is predicted that the quantized nature of electron thermal conductance survives up to room temperature, at which phonons already cease to exhibit thermal quantization, giving rise to high thermal conductance. In other words, the contribution from electrons to thermal conductance is negligible compared to that from phonons at moderate temperatures. In **Figure 3**, the temperature dependence of the ratio of thermal conductance $\kappa_{\mathrm{el}}/\kappa_{\mathrm{ph}}$ for electrons and phonons is illustrated. The experimentally observed ratio [20] is 1 order of magnitude lower than the present value. The discrepancy is attributed to the theoretical treatment of SWCNTs as purely metallic, whereas only a certain fraction $(\sim 1/3)$ [5, 11] of the crystalline ropes of SWCNTs in the experiment will be metallic and contribute to $\kappa_{\mathrm{el}}$.

### 2.2. Carbon nanotube as phonon waveguide

In this subsection, nonequilibrium molecular dynamics (NEMD) simulations are carried out with the Brenner bond-order potential for carbon-carbon covalent bonds [21] and the Lennard-Jones one for van der Waals interaction between the tube walls [22]. In our NEMD simulations, different temperatures, $T_{\mathrm{C}}$ $(= 290\ \mathrm{K})$ and $T_{\mathrm{H}}$ $(= 310\ \mathrm{K})$, are assigned to several layers of the left- and right-hand sides of a SWCNT. This leads to a thermal current from the right to left through the SWCNT, as shown in **Figure 4**. The Nosé-Hoover thermostat is utilized to control the temperature of the left and right-hand side several layers [24, 25], and we impose the fixed boundary condition, so that the edge atoms of SWCNTs are fixed rigidly. The length of the

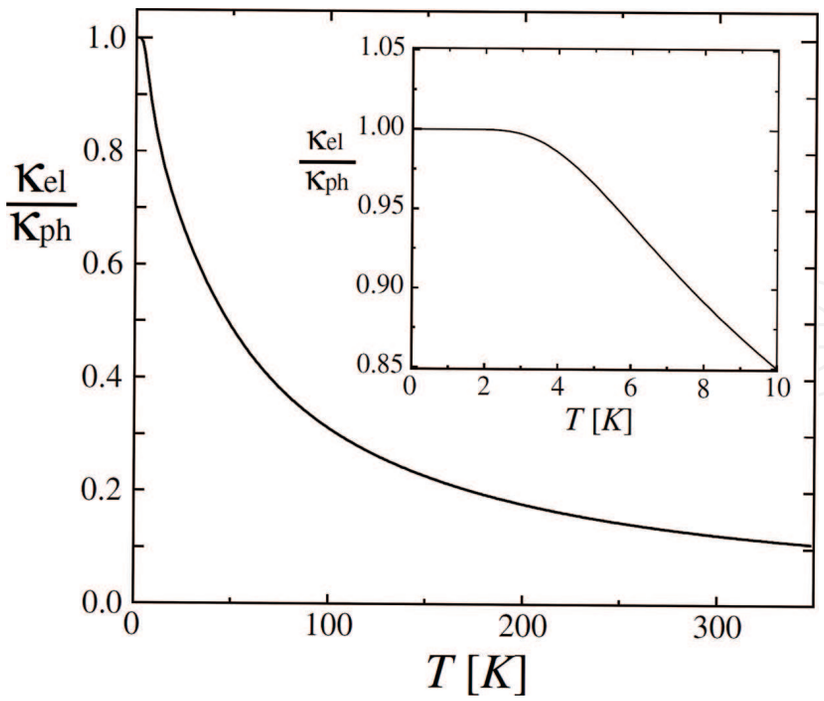


**Figure 3.** Ratio of thermal conductance by electrons, to that by phonons for a (10,10) SWCNT [6]. The inset gives results at low temperatures on an expanded scale. Copyright 2004 American Physical Society.

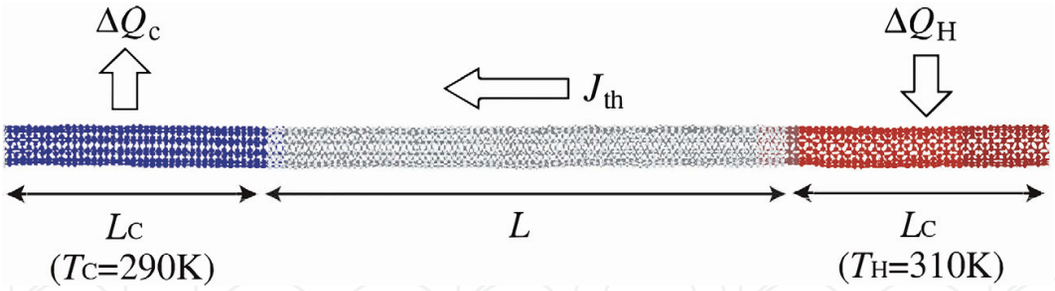


**Figure 4.** Schematic of the SWCNT in which different temperatures are assigned to the left- and right-end several layers [23]. Copyright 2009 the Japan Society of Applied Physics.

temperature-controlled layers is taken to be $L_C = L/2$, where $L$ is the length of the phonon-conduction region. The tunable parameters in the Nosé-Hoover thermostat method were optimized so as to minimize contact thermal resistance [26]. In our simulations, we solve Hamilton's classical equations of motion using second-order operator splitting integrators [27] with the molecular-dynamics (MD) time step of 0.5 fs.

In this subsection, the thermal conductance $\kappa$ is treated as

$$\kappa = \frac{J_{\text{th}}}{T_{\text{H}} - T_{\text{C}}} \tag{6}$$

Here, the steady-state thermal current, $J_{\text{th}}$, is calculated as follows:

$$J_{\text{th}} = \frac{\sum_{j=1}^{n} [\Delta Q_{\text{H}}(j) - \Delta Q_{\text{C}}(j)]}{2n\Delta t} \tag{7}$$

where $n$ represents the number of MD steps and $-\Delta Q_{\text{H(C)}}(j)$ is the amount of heat added to the right temperature-controlled layers (removed from the left ones) per unit time (see **Figure 4**).

First, the influence of bending deformation on the thermal conductance of SWCNTs is discussed. In our simulations, shortening the distance between the two ends of a SWCNT realizes bending. The right panels (a)-(c) in **Figure 5** illustrate the bent $(5,5)$ SWCNT for compression lengths $l_{\text{comp}} = 0, 60,$ and 120 nm, respectively. It can be seen that the CNT is severely bent as the edge-layer distance decreases. In the simulations, the bending deformation arises from stretching of carbon-carbon bond lengths, and the hexagonal network of carbon atoms in the SWCNT is not broken. The left panel in **Figure 5** shows the thermal conductance of the $(5,5)$ SWCNT with $L = 100$ nm as a function of the compression length. Our simulations exhibits that the bending does not affect the thermal conductance. Although the value of thermal conductance depends on $L$, the $L$-dependence is not discussed here because the conclusion of the study does not change qualitatively within the range from $L = 100$ to 250 nm as calculated. For the $L$-dependence, we refer the reader to other published papers [26, 28–31].

The bending robustness of $\kappa$ can be understood through a perspective of the phonon dispersion relations as shown in **Figure 6**, given by the power spectra of velocity fluctuations calculated by MD simulations [26, 28]. **Figure 6(a)-(c)** show the dispersion relations of the bent

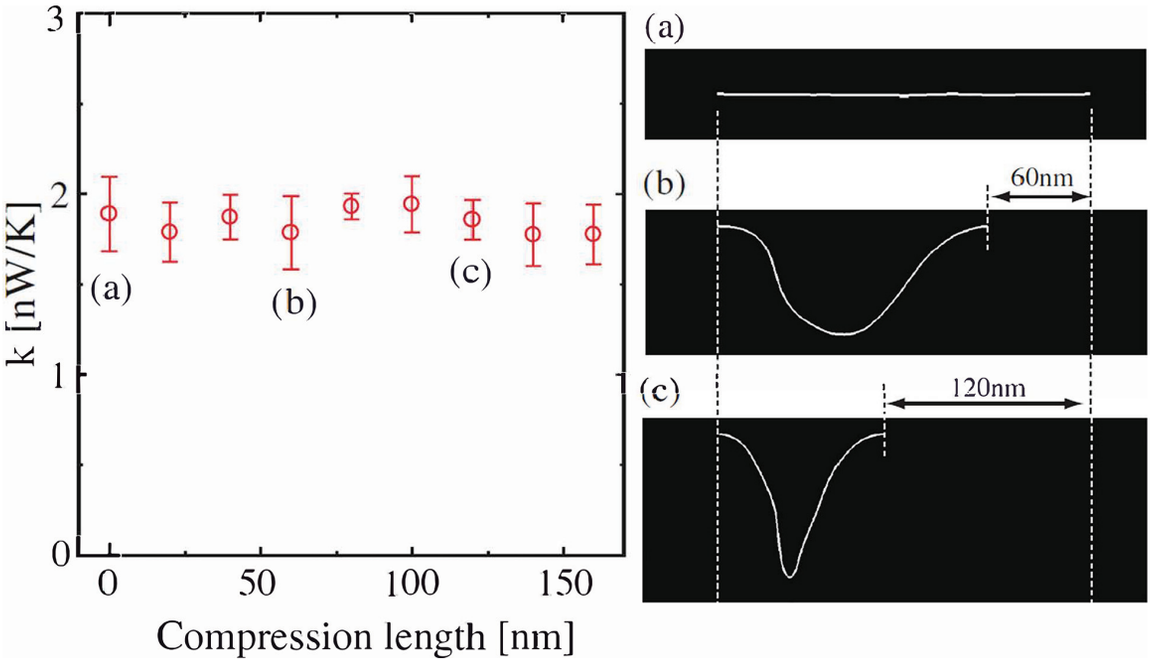


**Figure 5.** The thermal conductance of the (5,5) SWCNT with 200 nm length as a function of the compression length [23]. The right panels (a)–(c) represent the MD snapshots of a bended CNT. Copyright 2009 the Japan Society of Applied Physics.

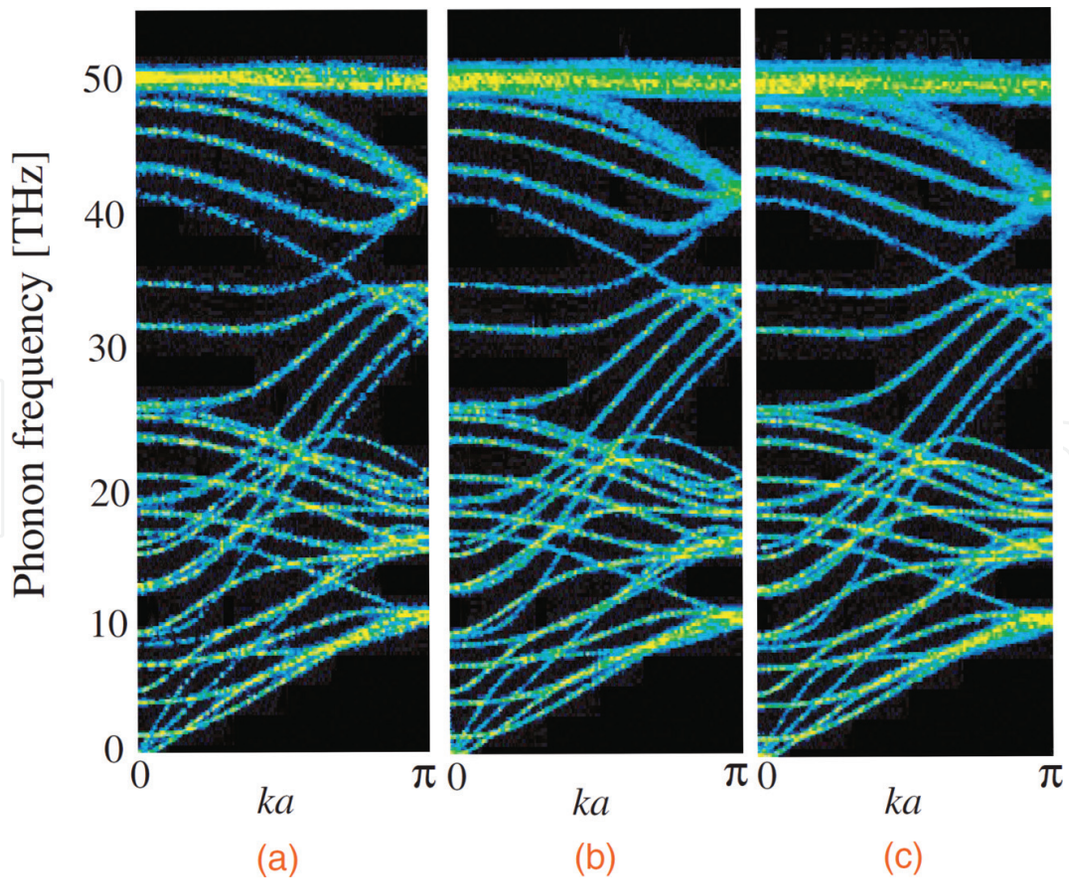


**Figure 6.** The phonon dispersion relations of the (5,5) SWCNT with the compression length (a) 0, (b) 60, and (c) 120 nm [23]. Copyright 2009 the Japan Society of Applied Physics.

$(5,5)$ SWCNT for $l_{\text{comp}} = 0, 60,$ and 120 nm, respectively. Since the bending deformation does not break the hexagonal network of the SWCNT is not broken by the bending deformation, a change of the dispersion structure due to the bending is very small. More specifically, the dispersion structure in the low-energy region remains unchanged after the bending, whereas that in the high-frequency region is slightly changed as shown in **Figure 6**. Consequently, $\kappa$ at the room-temperature is unaffected by the local bond-length deformation due to the bending. The bending robustness obtained by our simulations supports the experimental results of Chang et al. [32].

### 2.3. Phonon Anderson localization in isotope-disordered carbon nanotube

This subsection is focused on the interference effects of coherent phonons in SWCNTs. Here, we performed calculations for two typical examples: a (5,5) metallic SWCNT with 15.0% $^{13}$C and a (8,0) semiconducting SWCNT with 9.4% $^{14}$C. Our simulation is based on the Landauer theory of phonon transport combined with the nonequilibrium Green's function (NEGF) technique [33–35]. We used the Brenner bond-order potential for the interaction between carbon atoms [21], as used in the previous subsection. It is assumed that isotope disorder exists only in a central region with a length $L$. This region is connected to semi-infinite pristine SWCNT leads, not including any defects or impurities (**Figure 7**). In accordance with the Landauer theory within the linear response with the temperature difference between hot and cold baths [1], the phonon derived thermal conductance can be expressed as $\kappa(T) = \int_0^\infty \frac{d\omega}{2\pi} \hbar\omega \frac{\partial f_B(\omega,T)}{\partial T} \langle \zeta(\omega) \rangle$, where s $\hbar$ is Planck's constant, $T$ is the average temperature of the hot and cold baths, $f_B(\omega, T)$ is the Bose-Einstein distribution function for a phonon with a frequency $\omega$ in the baths, and $\langle \zeta(\omega) \rangle$ is the phonon-transmission function averaged over an ensemble of samples with different isotope configurations. We adopted over 200 realizations for each $L$ at each $\omega$.

In the NEGF technique, the phonon-transmission function $\zeta(\omega)$ is given by $\zeta(\omega) = \text{Tr}[\boldsymbol{\Gamma}_L(\omega) \boldsymbol{G}(\omega) \boldsymbol{\Gamma}_R(\omega) \boldsymbol{G}^\dagger(\omega)]$, where $\boldsymbol{G}(\omega) = \left[\omega^2 \boldsymbol{M} - \boldsymbol{D} - \boldsymbol{\Sigma}_L(\omega) - \boldsymbol{\Sigma}_R(\omega)\right]^{-1}$ is the retarded Green's function in the central region and $\boldsymbol{\Gamma}_{L(R)}(\omega) = i\left(\boldsymbol{\Sigma}_{L(R)}(\omega) - \boldsymbol{\Sigma}^\dagger_{L(R)}(\omega)\right)$ is the level broadening function due to the left (right) lead [33–35]. Here, $\boldsymbol{D}$ is a dynamical matrix in the central region, $\boldsymbol{M}$ a diagonal matrix with elements corresponding to the masses of the constituent atoms, and $\boldsymbol{\Sigma}_{L(R)}(\omega)$ a self-energy due to the left (right) lead. A merit of NEGF technique is that the phonon transport in micrometer-length nanotubes can be efficiently computed. We can easily calculate the statistical average of the phonon transmission for nanotubes within the wide range of tube

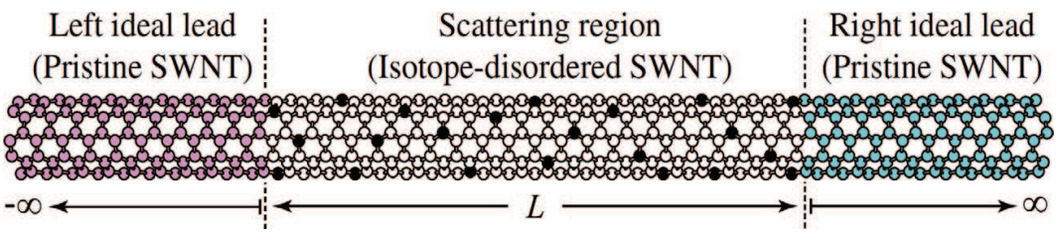


**Figure 7.** Schematic of an isotope-disordered SWCNT [36]. Copyright 2011 American Physical Society.

length with respect to huge number of isotope configurations. On the other hand, consideration of many-body interactions such as phonon-phonon scattering requires much computation time in the NEGF technique.

To perform the NEGF simulations, we first optimized the structures of a pristine (5,5) metallic and (8,0) semiconducting SWCNTs, and then calculated $\boldsymbol{D}$ from the second derivative of the total energy of the optimized structures with respect to the atom coordinate. By using $\boldsymbol{D}$ and the recursion method, we can easily compute $\boldsymbol{\Sigma}_{L(R)}(\omega)$. Moreover, we assume that the isotopes are taken into account only in $\boldsymbol{M}$.

Coherent-phonon transport is classified into three regions based on a relation among the length $L$ of the central region: the ballistic regime for $L \ll l_{\mathrm{MFP}}(\omega)$, the diffusive one for $l_{\mathrm{MFP}}(\omega) \ll L \ll \xi(\omega)$, and the localization one for $L \gg \xi(\omega)$. Here, $l_{\mathrm{MFP}}(\omega)$ is the mean free path and $\xi(\omega)$ the localization length. Before discussing the phonon-transmission histogram, we first determine $l_{\mathrm{MFP}}(\omega)$ and $\xi(\omega)$ for isotope-disordered SWCNTs. We adopt the procedure used in Ref. [37] to estimate these lengths. **Figure 8(a)** shows the average phonon transmission $\langle\zeta(\omega)\rangle$ of the (5,5) SWCNT with 15% $^{13}$C for various $L$ up to 5 m. In the very low-frequency region, $\langle\zeta(\omega)\rangle$ does not decrease and is almost four, even in the presence of isotope impurities. Perfect transmission (i.e., ballistic transport) is realized because the wavelength of acoustic phonons in the low-$\omega$ region is much longer than $L$. The Landauer expression of thermal conductance eventually exhibits universal quantization of $4\kappa_0$ at low temperatures irrespective of the presence and absence of isotope impurities (the factor 4 reflects the number of acoustic phonon modes).

In contrast, $\langle\zeta(\omega)\rangle$ decreases rapidly in the higher frequency region with increasing $L$, as shown in **Figure 8(a)**. There are two possible mechanisms for the reduction of $\langle\zeta(\omega)\rangle$: diffusive scattering and phonon localization. For the former, $\langle\zeta(\omega)\rangle$ decreases with $L$ according to $\langle\zeta(\omega)\rangle = M(\omega)/(1 + L/l_{\mathrm{MFP}}(\omega))$, where $M(\omega)$ means the number of phonon modes. On the other hand, for the latter mechanism, the phonon-transmission function decays exponentially with $L$ according to the scaling law $\langle \ln\zeta(\omega)\rangle = -L/\xi(\omega)$. In other words, $\xi(\omega)$ is defined by the scaling law. To clarify these mechanisms for the phonon-transmission reduction, the $L$-dependences of $\langle\zeta(\omega)\rangle$ and $\langle \ln\zeta(\omega)\rangle$ are plotted in **Figure 8(b)** and **(c)** for the two mechanisms, respectively. As **Figure 8(b)** shows that the numerical data of $\langle\zeta(\omega)\rangle$ at $\omega = 34\ \mathrm{cm}^{-1}$ and $391\ \mathrm{cm}^{-1}$ are well fitted by the dashed lines. In particular, the slope of the dashed line for $\omega = 34\ \mathrm{cm}^{-1}$ is almost zero, implying that $l_{\mathrm{MFP}}$ is very long and the phonon transport is ballistic at this frequency, as has been discussed above. For $\omega = 391\ \mathrm{cm}^{-1}$, the slope is finite, which indicates that phonon transport at this frequency is in the diffusive regime. In contrast to the low frequencies, at higher frequencies ($\omega = 1071$,1207, and $1513\ \mathrm{cm}^{-1}$), the calculated values deviate from the dashed lines with increasing $L$, although they are well fitted in the short-$L$ region. This deviation means that the phonon-transmission reduction for high-$\omega$ phonons of a long-$L$ SWCNT cannot be explained by the diffusive scattering mechanism. As shown in **Figure 8(c)**, the data for $\omega = 1071$,1207, and $1513\ \mathrm{cm}^{-1}$ are well fitted by the dashed lines in the $\langle \ln\zeta\rangle$ plot. Thus, it can be concluded that phonon localization causes the phonon-transmission reduction for high-$\omega$ phonons in a long-$L$ SWCNT.

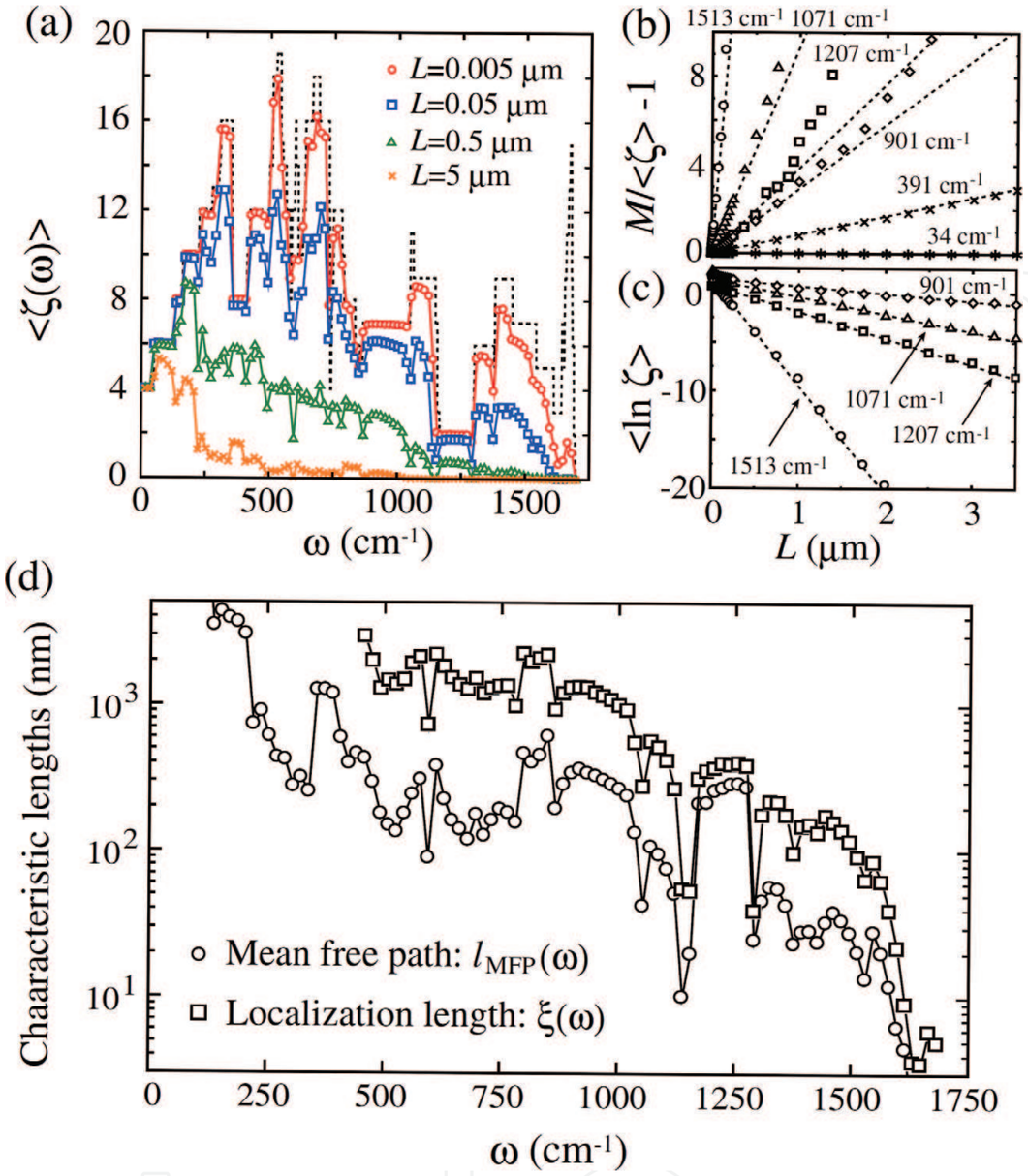


**Figure 8.** (a) The average phonon transmission of the (5,5) SWCNT with 15% $^{13}$C [36]. (b) The length dependence of the transmission for estimating the mean free path and (c) for the localization length. (d) The mean free path and the localization length as functions of frequency. Copyright 2011 American Physical Society.

$l_{\mathrm{MFP}}$ and $\xi(\omega)$ can be estimated from the slope of dashed lines in **Figure 8(b)** and **(c)**, respectively. The estimated $l_{\mathrm{MFP}}$ and $\xi(\omega)$ for the (5,5) SWCNT with 15% $^{13}$C are presented in **Figure 8(d)**. This result is in excellent agreement with the phenomenological Thouless relation, $\xi(\omega) = (M(\omega)+1)l_{\mathrm{MFP}}(\omega)/2$, similar to electron systems with time-reversal symmetry [38]. Thus, the three distinct regimes (ballistic, diffusive, and localization) could be clarified.

**Figure 9** shows the $^{13}$C-concentration dependence of $\kappa(T)$ in the (8,0) semiconducting SWCNT with 2 μm length at 300 K. As seen in **Figure 9**, thermal conductance decreases rapidly as the concentration increases. When the concentration overs about 20%, $\kappa(T)$ decreases by 80% in comparison with the pristine (8,0) SWCNT.

We now discuss the phonon-transmission fluctuation, defined by a standard deviation $\Delta\zeta(\omega) \equiv \sqrt{\left\langle \zeta(\omega)^2 \right\rangle - \langle \zeta(\omega) \rangle^2}$. **Figure 10** shows $\Delta\zeta(\omega)$ for (a) 625 nm-long (5,5) SWCNT with 15% $^{13}$C and (b) 210 nm-long (8,0) SWCNT with 9.4% $^{14}$C. The fluctuation of a physical quantity generally decreases as its average value increases. However, the fluctuation of phonon transmission is constant within the frequency region in the diffusive regime although $\langle \zeta(\omega) \rangle$ varies depending on $\omega$ [see also **Figure 8(a)**]. The constant value is estimated to be $\Delta\zeta(\omega) = 0.35 \pm 0.02$ and indicated by the dashed lines in **Figure 10(a)** and **(b)**. Thus, $\Delta\zeta(\omega)$ in the diffusive regime is universal and is independent of the background phonon transmission, the tube chirality and length, the isotope concentration, and the type of isotopes. This universal fluctuation is realized only in the diffusive regime and not in the ballistic and localization regimes. Interestingly, the value of $\Delta\zeta(\omega) = 0.35 \pm 0.02$ is the same as the value of the universal conductance fluctuation (UCF) for coherent electron transport in disordered quasi-1D systems,

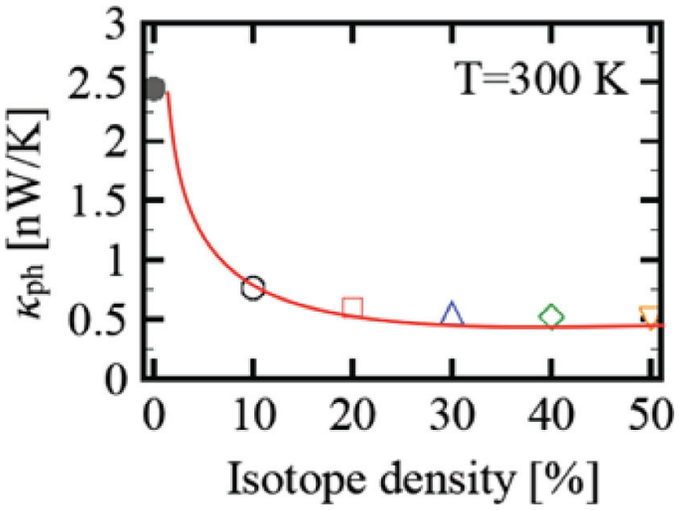


**Figure 9.** $^{13}$C-concentration dependence of thermal conductance of the (8,0) SWCNT with 2 μm length at 300 K.

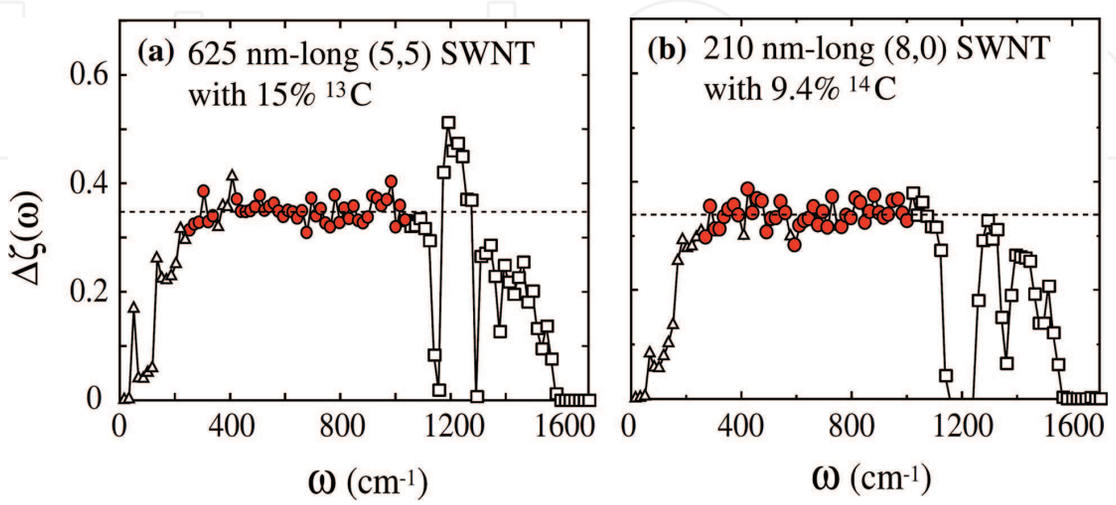


**Figure 10.** The root-mean-square phonon transmission for (a) the (5,5) SWCNT and (b) the (8,0) SWCNT [36]. Copyright 2011 American Physical Society.

$\Delta G/G_0 = 0.365$, within the statistical error. Here, $G_0$ and $\Delta G$ are respectively the electrical conductance quantum and the electrical conductance fluctuation. This means that the universal phonon-transmission fluctuation is closely related to the UCF even though electrons and phonons obey different quantum statistics. Similar to the UCF, the reason for the macroscopically observable phonon-transmission fluctuation can be qualitatively understood as follows: the fluctuations of phonon-transmission channels cannot cancel each other because there are very few effective transmission channels due to isotope scattering. To obtain a quantitative and complete understanding of the universal phonon-transmission fluctuation, some sophisticated microscopic theories are required.

In the final of this subsection, we discuss the phonon-transmission histogram $P(\zeta)$ that contains information for every moment of $\zeta(\omega)$. In **Figure 11(a)** and **(b)**, $P(\zeta)$ for several typical frequencies in the diffusive regime of (a) 625 nm-long (5,5) SWCNT with 15% $^{13}$C and (b) 210 nm-long (8,0) SWCNT with 9.4% $^{14}$C are shown. All the histograms in these figures are well described by a Gaussian distribution function with the universal fluctuation

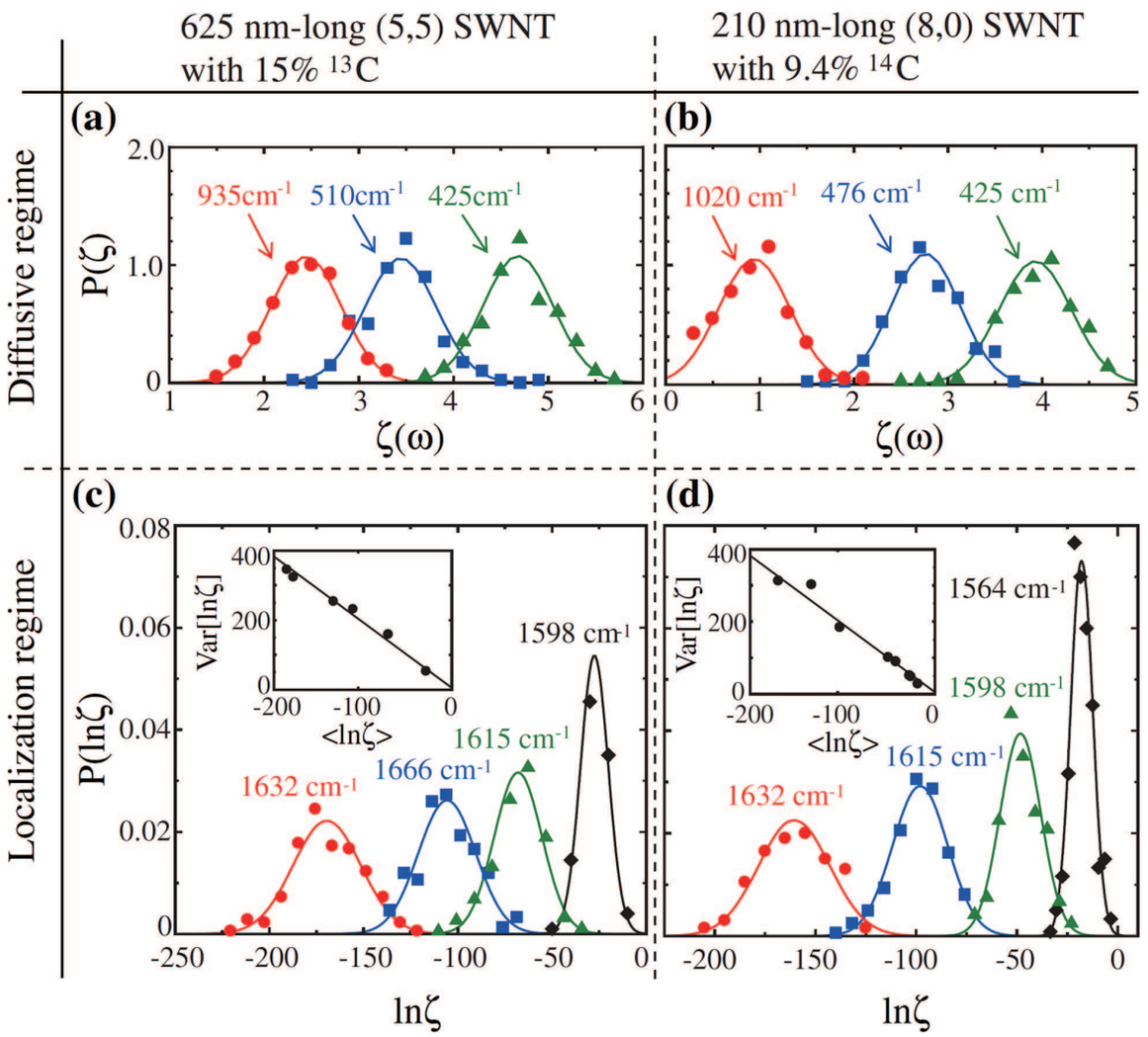


**Figure 11.** Phonon-transmission histograms for several frequencies in the diffusive regime for (a) the (5,5) SWCNT and (b) the (8,0) SWCNT, and in the localization regime for (c) the (5,5) SWNT and (d) the (8,0) SWCNT [36]. The insets show the variance. Copyright 2011 American Physical Society.

| Phonon transport regime | Phonon-transmission histogram | Average | Standard deviation |
|---|---|---|---|
| Ballistic regime ($L \ll l_{MFP}$) | Nearly delta function | $\sim M(\omega)$ | $\sim 0$ |
| Diffusive regime ($l_{MFP} \ll L \ll \xi$) | Gaussian distribution | Power-law decay with $L$ | Universal ($\sim 0.35 \pm 0.02$) |
| Localization regime ($L \gg \xi$) | Lognormal distribution | Exponential decay with $L$ | Decreases as $\langle \ln \zeta \rangle$ |

**Table 1.** Phonon-transmission histogram in ballistic, diffusive, and localization regimes [36]. Copyright 2011 American Physical Society.

$\Delta\zeta(\omega) = 0.35 \pm 0.02$. This is similar to the fact that the electrical conductance histogram in the diffusive region is expressed by a Gaussian distribution function with the UCF [38].

In $L \gg \xi(\omega)$ regime, $P(\zeta)$ becomes no longer a symmetric Gaussian distribution. By analogy with the electrical conductance histogram in the localization regime [39], one can easily expect that the asymmetric histogram is a lognormal function of $\zeta$. In fact, $P(\ln \zeta)$ can be well described by a Gaussian distribution as shown in **Figure 11(c)** and **(d)**. Unlike the other regimes, the variance $\mathrm{Var}[\ln \zeta] \equiv (\Delta \ln \zeta)^2$ of $P(\ln \zeta)$ decreases with increasing $\langle \ln \zeta \rangle$ according to $\mathrm{Var}[\ln \zeta] \sim -2\langle \ln \zeta \rangle$ as shown in the insets of these figures, similar to the situation for electrons [38]. The transmission fluctuation in the localization regime is material independent in the sense that the slope of $\mathrm{Var}[\ln \zeta]$ does not depend on the tube geometry, isotope concentration, or the type of isotopes. The above-mentioned results for the ballistic, diffusive, and localization regimes are summarized in **Table 1**.

## 3. Crossover from ballistic to diffusive phonon transport

This section discusses the crossover from ballistic to diffusive phonon transport in SWCNT using some basic arithmetic which follows from the fictitious-probe idea. In this idea, the thermal conductance was found to formally have the same expression as the Landauer formula for coherent phonon transport [1, 6]:

$$\kappa = \sum_{\nu} \int_{\omega_\nu^{\min}}^{\omega_\nu^{\max}} \frac{d\omega}{2\pi} \hbar\omega \left[ \frac{\partial f(\omega, T)}{\partial T} \right] T_\nu(\omega) \tag{8}$$

even when phonon-phonon scattering exists. Here, $T$ is an averaged temperature as descried in the previous section, and $T_\nu(\omega)$ is a phonon transmission function, effectively including the phonon-phonon scattering given as

$$T_\nu(\omega) = \zeta_\nu^{LR}(\omega) + \frac{\zeta_\nu^{FL}(\omega)\zeta_\nu^{FR}(\omega)}{\zeta_\nu^{LF}(\omega) + \zeta_\nu^{FR}(\omega)} \tag{9}$$

where $\zeta_\nu^{\alpha\beta}(\omega)$ is the transmission function of a coherent phonon with a phonon mode $\nu$ and frequency $\omega$ flowing from $\alpha$ to $\beta$ leads. Note that the inelastic component of thermal conductance in Eq. (8) is neglected, because it negligibly contributes to $\kappa$ of CNTs in the quasiballistic regime.

Thus far, we have discussed the role of a single probe with temperature $T_F$ . Generally, a spatial distribution of temperature exists inside the conductor. In order to incorporate this distribution, a conductor attaching $N$ probes in series, with respective temperatures $T_i (i = 1, 2\cdots, N)$ is introduced. For $N$ probes, the transmission function $T_\nu^{\mathrm{tot}}(\omega)$ propagating in a conductor of length $L$ can be written as

$$T_\nu^{\mathrm{tot}}(\omega) = \frac{L_\nu(\omega)}{L + L_\nu(\omega)} \sim \frac{\Lambda_\nu(\omega)}{L + \Lambda_\nu(\omega)} \tag{10}$$

where the characteristic length $L_\nu(\omega) \equiv T_\nu/\rho(1 - T_\nu)$ is expressed by the density of scatters in the conductor, $\rho = N/L$ and $T_\nu$. The derivation process of Eq. (10) is analogous to that of effective transmission for inelastic electronic transport in mesoscopic conductors [40]. Here, it is explained that we can regard $L_\nu(\omega)$ in Eq. (10) as the mean free path $\Lambda_\nu(\omega) = \tau_\nu(\omega)|v_\nu(\omega)|$, where $\tau_\nu(\omega)$ and $v_\nu(\omega)$ are the backscattering time and group velocity of a phonon with $\{\nu, \omega\}$, respectively. For phonon propagation over the distance between neighboring probes $dL \equiv L/N = 1/\rho$, the reflection probability $R_\nu(\omega)$ is given by $R_\nu(\omega) = (dL/|v_\nu(\omega)|)/\tau_\nu(\omega)$ $= 1/\rho\Lambda_\nu(\omega)$. Thus, the phonon's mean free path is $\Lambda_\nu(\omega) = 1/\rho R_\nu(\omega)$, and $L_\nu(\omega) \sim \Lambda_\nu(\omega)$ in the large-$N$ (or small-$dL$) limit where the transmission probability of each small segment with length $dL$ is close to one ($T_\nu(\omega) \sim 1$).

According to the above discussion, a general expression of thermal conductance is given as

$$\kappa = \sum_\nu \int_{\omega_\nu^{\min}}^{\omega_\nu^{\max}} \frac{d\omega}{2\pi} \hbar\omega \left[\frac{\partial f(\omega, T)}{\partial T}\right] \frac{\Lambda_\nu(\omega)}{L + \Lambda_\nu(\omega)} \tag{11}$$

For a short conductor ($L \ll \Lambda_\nu(\omega)$), Eq. (11) reproduces the Landauer formula [1, 6] for coherent phonon transport with perfect transmission. In the other limit ($L \gg \Lambda_\nu(\omega)$), it reduces to the Boltzmann-Peierls formula [41].

We now apply the developed formula (11) to thermal transport in SWCNTs at room temperature. Instead of estimating $\Lambda_\nu(\omega)$ from Eq. (9), we use an phenomenological expression $\Lambda_\nu(\omega) = c_\nu A/\omega^2 T$ for three-phonon Umklapp scattering events in the low-frequency limit $\hbar\omega/k_B T \ll 1$, where $A = 3.35 \times 10^{23}$ mK/s$^2$ is the coupling constant for graphene [42] and $c_\nu$ represents the curvature effect of a CNT ($c_\nu = 1$ corresponds to a graphene). By using this expression we can perform integration in Eq. (11) analytically. Strictly speaking, this expression can apply only to acoustic phonon modes with linear dispersion, but it has been shown to be useful to represent other modes as well [30]. Consequently, the thermal conductance is expressed simply as:

$$\kappa_{\mathrm{CNT}} = \frac{k_B}{2\pi} \sum_\nu \Omega_\nu \left\{ \arctan\left(\frac{\omega_\nu^{\max}}{\Omega_\nu}\right) - \arctan\left(\frac{\omega_\nu^{\min}}{\Omega_\nu}\right) \right\} \tag{12}$$

where $\Omega_\nu(L) = \sqrt{c_\nu A/TL}$ is an $L$-dependent characteristic frequency, which is a key quantity for understanding the crossover between ballistic and diffusive phonon transport in the CNTs. The $\nu$ dependence of $c_\nu$ is neglected hereafter, i.e., the mode-dependent characteristic

frequency $\Omega_\nu(L)$ is replaced by $\Omega(L)$. In spite of the relative simplification, this works remarkably well to describe $L$ dependence of thermal conductance in the quasi-ballistic regime, as will be discussed below.

In Eq. (10), effects of phonon scattering at interfaces between a CNT and the left/right leads were not included. One of simple treatments of the interfacial thermal resistance is to introduce it by the following way: $\kappa^{-1} = \kappa_{\rm CNT}^{-1} + \kappa_{\rm int}^{-1}$. The interfacial resistance $\kappa_{\rm int}^{-1}$ can be decided by fitting experimental or numerical calculation data.

Now, we estimate the thermal conductance of SWCNTs by performing the NEMD simulations [26, 28] with Brenner's bond-order potential [21], and compare the MD results to the above-described theory. The $L$-dependence of thermal conductance was quantified for various tube lengths, up to micrometers at $T = 300$ K ($T_{\rm hot} = 310$ K and $T_{\rm cold} = 290$ K). We refer the detailed simulation procedure to Ref. [26]. The thermal conductances for (3,3) and (5,5) SWCNTs obtained from the NEMD simulations are shown by blue and red circles in **Figure 12**, respectively. The solid curves representing theoretical curves given the proper choice of two parameters $\kappa_{\rm int}$ and $c$ (e.g., $\kappa_{\rm int}^{-1} = 0.09$ K/nW and $c = 0.65$ for the (3,3) SWCNT) excellently agree with the MD data. Most recently, the $L$-dependent thermal conductance (or conductivity) of SWCNTs shown here has been measured in experiments [31, 44], although we cannot compare the theory with the experiments because the detailed information on tube structure such as number of walls and their chiralities was not described.

We return to discuss the ballistic-diffusive crossover. The relative position of $\Omega(L)$ with respect to the phonon dispersion relation determines the thermal-transport properties of SWCNTs. As illustrated in **Figure 13**, the dashed blue line indicates the position of $\Omega(L)$ relative to the

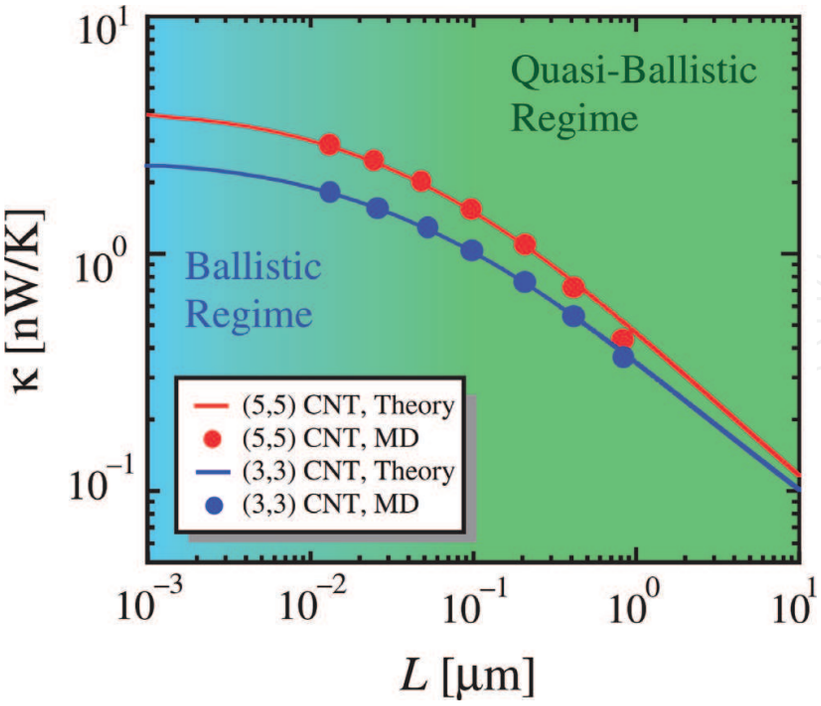


**Figure 12.** Length dependence of thermal conductance [43]. Copyright 2009 the Japan Society of Applied Physics.

http://dx.doi.org/10.5772/intechopen.81292

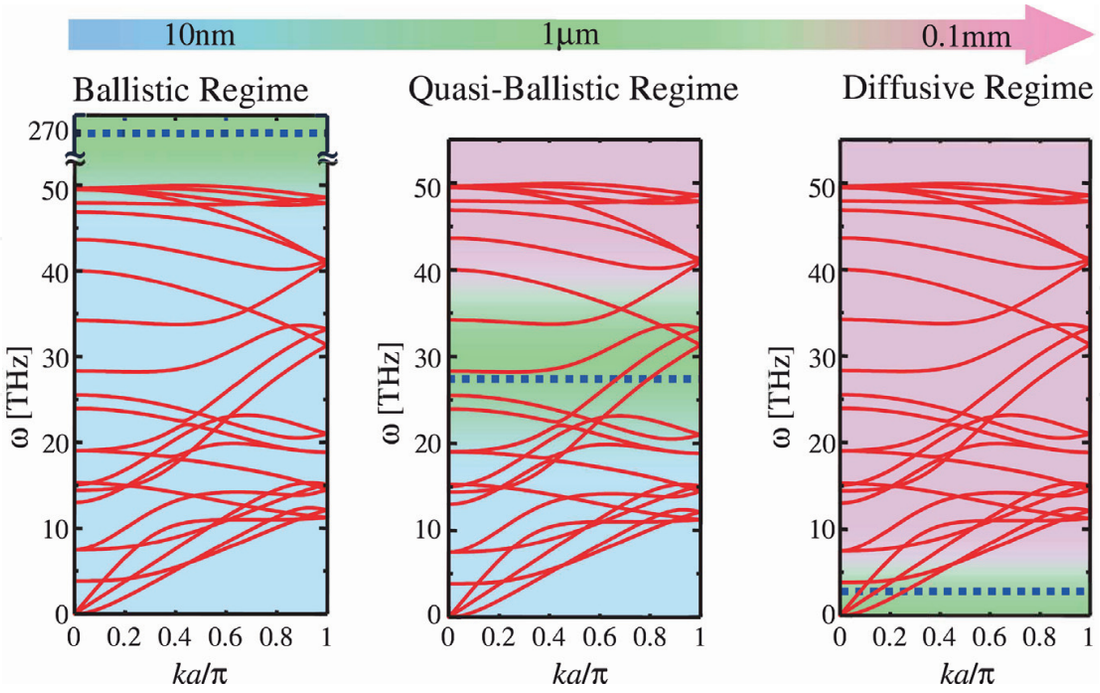


**Figure 13.** The relative position of the length dependent characteristic frequencies, 270 THz (left panel), 27 THz (middle panel), and 2.7 THz (right panel) [43]. Copyright 2009 the Japan Society of Applied Physics.

dispersion relation. As seen in **Figure 12**, nanometer-length SWCNTs display the thermal conductance independent of $L$, reflecting purely ballistic phonon transport. At nanometer length, $\Omega(L)$ is much larger than the energies of the phonons, as shown in the left panel of **Figure 13**.

With an increase in $L$, up to micrometer length, the value of $\Omega(L)$ decreases, lying in the middle of the phonon dispersion relation, as shown in the central panel of **Figure 13**. In this situation, low-frequency phonon modes ($\omega_\nu^{\max} \ll \Omega(L)$) give $L$-independent thermal conductance reflecting a ballistic nature, whereas the high-frequency modes $\left(\omega_\nu^{\min} \gg \Omega(L)\right)$ show $\kappa \propto 1/L$ reflecting a diffusive nature. The intermediate-frequency phonon modes ($\omega_\nu^{\min} < \Omega(L) < \omega_\nu^{\max}$) cannot be described in terms of both Landauer and Boltzmann-Peierls formulae, and the thermal conductance exhibits nonlinear $L$-dependence described by Eq. (12). Thus, it is concluded that micrometer-length SWCNTs belong to the quasi-ballistic thermal transport regime in which ballistic and diffusive phonons coexist.

Next, the case when $\Omega(L)$ is much lower than the excitation frequency of the lowest optical phonons is discussed, as shown in the right panel of **Figure 13**. In this case, the tube length$L$ reaches millimeters and the contribution of optical phonons to thermal conductance has a behavior as $\kappa \propto 1/L$, resulting in constant thermal conductivity, as $\lambda = (L/S)\kappa = \text{const}$. Here, $S$ is the cross-sectional area of a SWCNT. On the other hand, the acoustic modes show $\kappa \propto L^{-1/2}$, leading to a power-law divergence $\lambda \propto L^{1/2}$ of thermal conductivity [29, 30]. This divergence closely relates to the long-standing problem pointed out by Pomeranchuk in the 1940s that the low-frequency acoustic phonon contribution to thermal conductivity diverges in the thermodynamic limit $L \to \infty$ [45]. However, it is known, in general, that the divergence disappears if

we take into account higher-order phonon-phonon scattering events, although the possibility of the above-stated long-time tail in low-dimensional materials remains an open problem [46, 47]. In either case, the agreement between the current theory and MD simulation results indicates that the higher-order effects are negligible in the current length regime. This consists with the previously reported observation from Boltzmann's kinetic approach [30].

## 4. Thermal properties of graphene modulated by strain

Finally, we shortly mention the recent theoretical work about the thermal property in another carbon material, a graphene [48]. In this work, the strain response of the phonon specific heat was investigated. The low temperature behavior of the specific heat is dominated by the three acoustic modes, i.e., the longitudinal acoustic (LA) mode, transverse acoustic (TA) mode, and out-of-plane acoustic (ZA) mode. It is well known that the LA and TA modes have a linear dispersion in the long wavelength region while the other has a quadratic one in the absence of the strain [49]. This means that the ZA mode is critical for low-temperature dependence of the specific heat. As a result, the specific heat has a linear dependence at low temperature. As the strain increases, the dispersion of the ZA mode drastically changes, so that this dispersion becomes linear in the same as the LA and TA modes [50, 51]. Due to the ZA mode linearized by the strain, the low-temperature dependence of the specific heat becomes quadratic. Therefore, since the specific heat directly relates the thermal conductivity, it is easily expected that the strain can also modulate the temperature dependence of the thermal conductivity.

## 5. Conclusion

This chapter reviewed recent progress of theoretical studies on phonon transport in SWCNTs focusing on the quantization of phonon thermal conductance, phonon Anderson localization, and so on. At low temperature, the phonon thermal conductance of SWCNTs has a quantized universal value of $4\kappa_0$, where the factor, 4 is the number of the acoustic modes in SWCNTs. As the temperature increases, the crossover from the ballistic transport to diffusive one occurs and the thermal conductance in the intermediate region between them indicates the non-linear dependence of tube length.

## Acknowledgements

The authors would like to thank Kazuyuki Watanabe, Satoshi Watanabe, Shigeo Maruyama, Junichiro Shiomi, and Satoru Konabe for their useful discussions during this work. This work was supported, in part, by JSPS KAKENHI grants (nos. 19710083, 20048008, 22013004, 24681021, 15H03523 and 18H01816).

## Author details

Kenji Sasaoka[1] and Takahiro Yamamoto[2*]

*Address all correspondence to: takahiro@rs.tus.ac.jp

1 W-FST Center, RIST, Tokyo University of Science, Tokyo, Japan

2 Department of Liberal Arts, Faculty of Engineering, Tokyo University of Science, Tokyo, Japan

## References

[1] Rego LGC, Kirczenow G. Quantized thermal conductance of dielectric quantum wires. Physical Review Letters. 1998;**81**:232-235. DOI: 10.1103/Phys Rev Lett.81.232

[2] Angelescu DE, Cross MC, Roukes ML. Heat transport in mesoscopic systems. Superlattices and Microstructures. 1998;**23**:673-689. DOI: 10.1006/spmi.1997.0561

[3] Blencowe MP. Quantum energy flow in mesoscopic dielectric structures. Physical Review B. 1999;**59**:4992-4998. DOI: 10.1103/PhysRevB.59.4992

[4] Saito R, Takeya T, Kimura T, Dresselhaus G, Dresselhaus M S. Raman intensity of single-wall carbon nanotubes. Physical Review B. 1998;**57**:4145-4153. DOI: 10.1103/PhysRevB.57.4145

[5] Saito R, Dresselhaus G, Dresselhaus M S. Physical Properties of Carbon Nanotubes. London: Imperial College Press; 1998. DOI: 10.1016/S0921-5107(00)00444-X

[6] Yamamoto T, Watanabe S, Watanabe K. Universal features of quantized thermal conductance of carbon nanotubes. Physical Review Letters. 2004;**92**:075502. DOI: 10.1103/PhysRevLett.92.075502

[7] Dresselhaus M S, Dresselhaus G, Eklund P C. Science of Fullerenes and Carbon Nanotubes. New York: Academic; 1996

[8] Hone J, Llaguno MC, Biercuk MJ, Johnson AT, Batlogg B, Benes Z, et al. Thermal properties of carbon nanotubes and nanotube-based materials. Applied Physics A. 2002;**74**:339-343. DOI: 10.1007/s003390201277

[9] Hone J. Phonons and thermal properties of carbon nanotubes. In: Dresselhaus M S, Dresselhaus G, Avouris P, editors. Carbon Nanotubes: Synthesis, Structure, Properties, and Applications. Berlin: Springer-Verlag; 2001. pp. 273-287. DOI: 10.1007/3-540-39947-X

[10] Rego LGC, Kirczenow G. Fractional exclusion statistics and the universal quantum of thermal conductance: A unifying approach. Physical Review B. 1999;**59**:13080-13086. DOI: 10.1103/PhysRevB.59.13080

[11] Saito R, Fujita M, Dresselhaus G, Dresselhaus M S. Electronic structure of chiral graphene tubules. Applied Physics Letters. 1992;**60**:2204-2206. DOI: 10.1063/1.107080

[12] Hamada N, Sawada S, Oshiyama A. New one-dimensional conductors: Graphitic microtubules. Physical Review Letters. 1992;**68**:1579-1581. DOI: 10.1103/PhysRevLett.68.1579

[13] Dresselhaus MS, Jishi RA, Dresselhaus G, Inomata D, Nakano K, Saito R. Group theoretical concepts for carbon nanotubes. Molecular Materials. 1994;**4**:27-40

[14] Olk CH, Heremans JP. Scanning tunneling spectroscopy of carbon nanotubes. Journal of Materials Research. 1994;**9**:259-262. DOI: 10.1557/JMR.1994.0259

[15] Wildöer JWG, Venema LC, Rinzler AG, Smalley RE, Dekker C. Electronic structure of atomically resolved carbon nanotubes. Nature (London). 1998;**391**:59-62. DOI: 10.1038/34139

[16] Guttman GD, Ben-Jacob E, Bergman DJ. Thermoelectric properties of microstructures with four-probe versus two-probe setups. Physical Review B. 1996;**53**:15856. DOI: 10.1103/PhysRevB.53.15856-15862

[17] Greiner A, Reggiani L, Kuhn T, Varani L. Thermal conductivity and Lorenz number for one-dimensional ballistic transport. Physical Review Letters. 1997;**78**:1114-1117. DOI: 10.1103/PhysRevLett.78.1114

[18] Molenkamp LW, Gravier T, van Houten H, Buijk OJA, Mabesoone MAA, Foxon CT. Peltier coefficient and thermal conductance of a quantum point contact. Physical Review Letters. 2002;**68**:3765-3768. DOI: 10.1103/PhysRevLett.68.3765

[19] Rao AM, Richter E, Bandow S, Chase B, Eklund PC, Williams KA, et al. Dresselhaus diameter-selective Raman scattering from vibrational modes in carbon nanotubes. Science. 1997;**275**:187-191. DOI: 10.1126/science.275.5297.187

[20] Hone J, Whitney M, Piskoti C, Zettl A. Thermal conductivity of single-walled carbon nanotubes. Physical Review B. 1999;**59**:R2514-R2516. DOI: 10.1103/PhysRevB.59.R2514

[21] Brenner DW. Empirical potential for hydrocarbons for use in simulating the chemical vapor deposition of diamond films. Physical Review B. 1990;**42**:9458-9471. DOI: 10.1103/PhysRevB.42.9458

[22] Che J, Cagin T, Goddard WA III. Generalized extended empirical bond-order dependent force fields including nonbond interactions. Theoretical Chemistry Accounts. 1999;**102**:346-354. DOI: 10.1007/s002140050506

[23] Nishimura F, Takahashi T, Watanabe K, Yamamoto T. Bending robustness of thermal conductance of carbon nanotubes: Nonequilibrium molecular dynamics simulation. Applied Physics Express. 2009;**2**:035003. DOI: 10.1143/APEX.2.035004

[24] Nose S. A unified formulation of the constant temperature molecular dynamics methods. The Journal of Chemical Physics. 1984;**81**:511-519. DOI: 10.1063/1.447334

[25] Hoover WG. Canonical dynamics: Equilibrium phase-space distributions. Physical Review A. 1985;**31**:1695-1697. DOI: 10.1103/PhysRevA.31.1695

[26] Shiomi J, Maruyama S. Molecular dynamics of diffusive-ballistic heat conduction in single-walled carbon nanotubes. Japanese Journal of Applied Physics. 2008;**47**:2005-2009

[27] Tuckerman M, Berne BJ, Martyna GJ. Reversible multiple time scale molecular dynamics. The Journal of Chemical Physics. 1992;**97**:1990-2001. DOI: 10.1063/1.463137

[28] Maruyama S. A molecular dynamics simulation of heat conduction in finite length SWNTs. Physica B: Condensed Matter. 2002;**323**:193-195. DOI: 10.1016/S0921-4526(02)00898-0

[29] Wang J, Wang J–S. Carbon nanotube thermal transport: Ballistic to diffusive. Applied Physics Letters. 2006;**88**:111909. DOI: 10.1063/1.2185727

[30] Mingo N, Broid DA. Length dependence of carbon nanotube thermal conductivity and the problem of long waves. Nano Letters. 2005;**5**:1221-1225. DOI: 10.1021/nl050714d

[31] Chang CW, Okawa D, Garcia H, Majumdar A, Zettl A. Breakdown of Fourier's law in nanotube thermal conductors. Physical Review Letters. 2008;**101**:075903. DOI: 10.1103/PhysRevLett.101.075903

[32] Chang CW, Okawa D, Garcia H, Majumdar A, Zettl A. Nanotube phonon waveguide. Physical Review Letters. 2007;**99**:045901. DOI: 10.1103/PhysRevLett.99.045901

[33] Yamamoto T, Watanabe W. Nonequilibrium Green's function approach to phonon transport in defective carbon nanotubes. Physical Review Letters. 2006;**96**:255503. DOI: 10.1103/PhysRevLett.96.255503

[34] Mingo N. Anharmonic phonon flow through molecular-sized junctions. Physical Review B. 2006;**74**:125402. DOI: 10.1103/PhysRevB.74.125402

[35] Wang J-S, Wang J, Zeng N. Nonequilibrium Green's function approach to mesoscopic thermal transport. Physical Review B. 2006;**74**:033408. DOI: 10.1103/PhysRevB.74.033408

[36] Yamamoto T, Sasaoka K, Watanabe S. Universality and diversity in a phonon-transmission histogram of isotope-disordered carbon nanotubes. Physical Review Letters. 2011;**106**:215503. DOI: 10.1103/PhysRevLett.106.215503

[37] Savic´ I, Mingo N, Stewart DA. Phonon transport in isotope-disordered carbon and boron-nitride nanotubes: Is localization observable? Physical Review Letters. 2008;**101**:165502. DOI: 10.1103/PhysRevLett.101.165502

[38] Beenakker CW. Random-matrix theory of quantum transport. Review of Modern Physics. 1997;**69**:731-808. DOI: 10.1103/RevModPhys.69.731

[39] Imry Y. Active transmission channels and universal conductance fluctuations. Europhysics Letters. 1986;**1**:249-256. DOI: 10.1209/0295-5075/1/5/008

[40] Datta S. Electronic Transport in Mesoscopic Systems. Cambridge: Cambridge University Press; 1995

[41] Peierls RE, editor. Quantum Theory of Solid. New York: Oxford University Press; 1995

[42] Klemens PG, Pedraza DF. Thermal conductivity of graphite in the basal plane. Carbon. 1994;**32**:735-741. DOI: 10.1016/0008-6223(94)90096-5

[43] Yamamoto T, Konabe S, Shiomi J, Maruyama S. Crossover from ballistic to diffusive thermal transport in carbon nanotubes. Applied Physics Express. 2009;**2**:095003. DOI: 10.1143/APEX.2.095003

[44] Wang ZL, Tang DW, Li XB, Zheng XH, Zhang WG, Zheng LX, et al. Length-dependent thermal conductivity of an individual single-wall carbon nanotube. Applied Physics Letters. 2007;**91**:123119. DOI: 10.1063/1.2779850

[45] Pomeranchuk I. Heat conductivity of dielectrics at high temperatures. Journal of Physics (USSR). 1941;**4**:259

[46] Lepri S, Livi R, Politi A. Thermal conduction in classical low-dimensional lattices. Physics Report. 2003;**377**:1-80. DOI: 10.1016/S0370-1573(02)00558-6

[47] Livi R, Lepri S. Thermal physics: Heat in one dimension. Nature. 2003;**421**:327. DOI: 10.1038/421327a

[48] Tada K, Funatani T, Konabe S, Sasaoka K, Ogawa M, Souma S, et al. Modulations of thermal properties of graphene by strain-induced phonon engineering. Japanese Journal of Applied Physics. 2017;**56**:025102. DOI: 10.7567/JJAP.56.025102

[49] Carrete J, Li W, Lindsay L, Broido DA, Gallego LJ, Mingo N. Physically founded phonon dispersions of few- layer materials and the case of borophene. Materials Research Letters. 2016;**4**:204. DOI: 10.1080/21663831.2016.1174163

[50] Bonini N, Garg J, Marzari N. Acoustic phonon lifetimes and thermal transport in free-standing and strained graphene. Nano Letters. 2673;**2012**:12. DOI: 10.1021/nl202694m

[51] Ma F, Zheng HB, Sun YJ, Yang D, Xu KW. Strain effect on lattice vibration, heat capacity, and thermal conductivity of graphene. Applied Physics Letters. 2012;**101**:111904. DOI: 10.1063/1.4752010